



# Broadband modeling of the 2002 Denali fault earthquake on the Earth Simulator

Seiji Tsuboi<sup>a,\*</sup>, Dimitri Komatitsch<sup>b</sup>, Chen Ji<sup>b</sup>, Jeroen Tromp<sup>b</sup>

<sup>a</sup> Institute for Frontier Research on Earth Evolution, Japan Marine Science and Technology Center,  
3173-25 Showa-machi, Kanazawa-ku, Yokohama 236-0001, Japan

<sup>b</sup> Seismological Laboratory, California Institute of Technology, 1200 East California Boulevard, Pasadena, CA 91125, USA

Received 27 June 2003; accepted 15 September 2003

## Abstract

We use a spectral-element method implemented on the Earth Simulator in Japan to simulate broadband seismic waves generated by the 3 November 2002 Denali fault earthquake. This  $M_w = 7.9$  event is the largest strike–slip earthquake in North America in almost 150 years. The source model is constrained by teleseismic body waves and observed surface offsets. The earthquake was initiated by a small thrust event, and is well characterized by a five-segment fault geometry dominated by right-lateral rupture along 220 km of the Denali fault. We perform the three-dimensional numerical simulations at unprecedented resolution and reveal significantly enhanced ground motions (directivity) toward the conterminous United States for both body and surface waves.

© 2003 Elsevier B.V. All rights reserved.

*Keywords:* Broadband modeling; Denali fault; Earth Simulator; Spectral-element method

## 1. Introduction

Detailed mapping of the three-dimensional (3D) seismic velocity structure of the Earth is traditionally performed using a combination of short-period body and long-period surface waves. Modeling the rupture process during an earthquake also involves the analysis of both body and surface waves. Thus, the validation of 3D Earth models and finite-source models requires the ability to calculate accurate broadband seismograms, i.e. synthetic seismograms that contain both short-period body waves and long-period surface waves. Here we use the Earth Simulator located at the Japan Marine Science and Technology Center

(JAMSTEC) (<http://www.es.jamstec.go.jp>) to simulate broadband seismic waves generated by the  $M_w = 7.9$ , 3 November 2002 Denali fault earthquake at periods longer than 5 s in a fully 3D Earth model.

## 2. Source model

The main rupture occurred on the dextral Denali fault, which has been active since the late Cretaceous in response to the oblique convergence between the North American plate and the Pacific plate (Page et al., 1995). This tectonic setting dictates that the motion is dominated by right-lateral strike–slip. We constructed a five-segment fault geometry using observed surface offsets (Eberhart-Phillips et al., 2003) and teleseismic body-wave recordings as constraints (Ji et al.,

\* Corresponding author. Fax: +81-45-778-5439.  
E-mail address: [tsuboi@jamstec.go.jp](mailto:tsuboi@jamstec.go.jp) (S. Tsuboi).

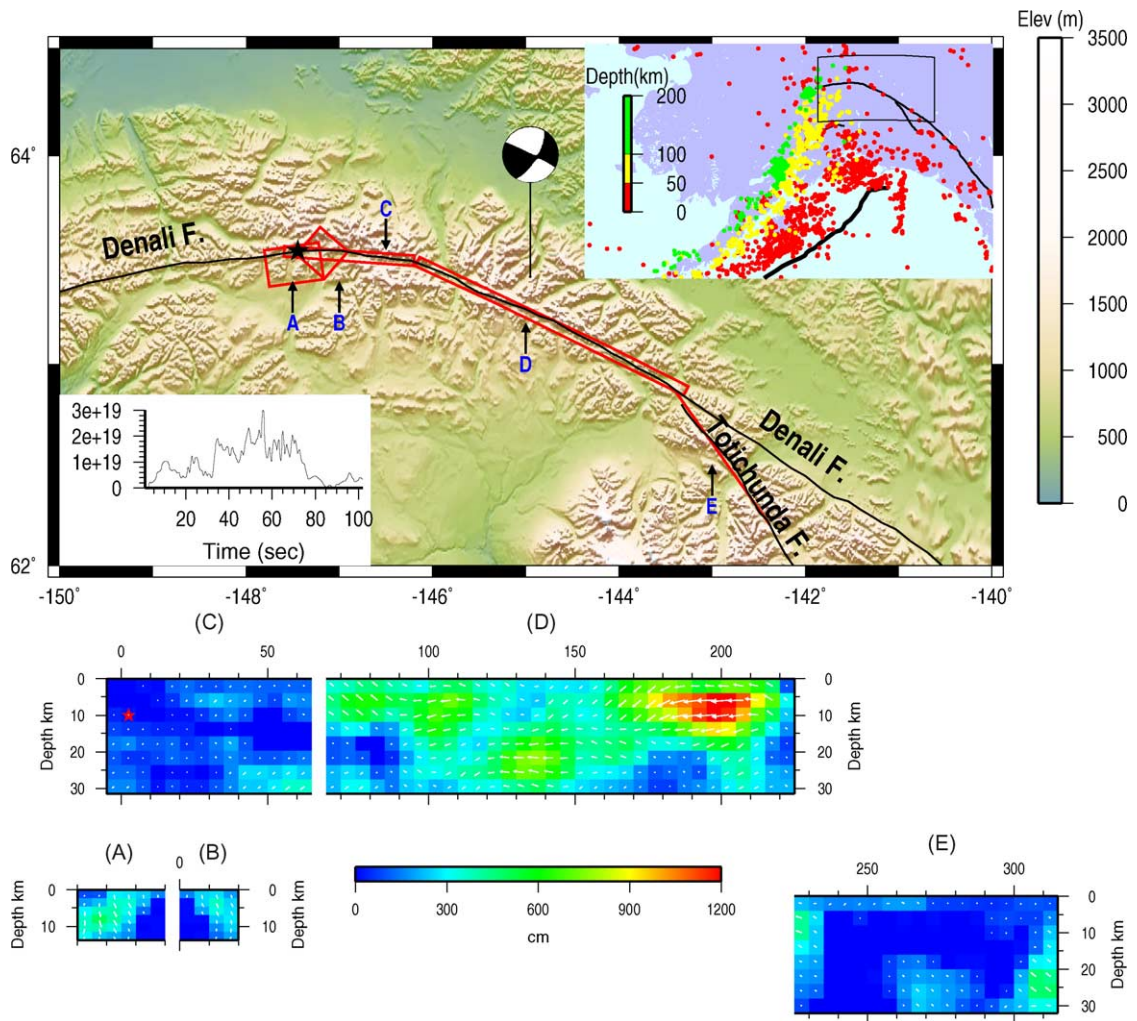


Fig. 1. (Top) Fault geometry of the 3 November 2002, Denali fault earthquake. The top-right inset shows a map on which relocated seismicity determined by the International Seismological Center (Engdahl et al., 1998) is color-coded according to hypocentral depth. The thick black line off the coast denotes the location of the Aleutian trench. The black box denotes the area of detail shown in the larger map, on which the Denali and Totichunda faults are labeled. The Harvard Centroid-Moment Tensor solution (<http://www.seismology.harvard.edu>) is shown by the black-and-white beach ball. The five red boxes labeled A–E denote the surface projections of the five fault segments that were involved in the rupture. The earthquake started at the black star with a thrust event represented by fault planes A and B, which both have a  $32^\circ$  dip to the North, and Northwest, respectively. The rupture then proceeded as strike-slip motion along the nearly vertical fault planes C, D and E. Segments C and D represent the main rupture along the Denali fault, whereas segment E represents the rupture along the Totichunda fault. The average moment-rate function is plotted as a function of time in the bottom left corner of the map. (Bottom) Slip distribution along the five fault segments A–E shown in the top. The red star on segment C denotes the point of rupture initiation. This point is shared with fault planes A and B. The white arrows on the fault plane denote the slip direction, and their length is proportional to the amount of slip.

2002a) (Fig. 1). The body waves are used to reconstruct the slip history, slip vector, rupture initiation time, and width of an analytic slip-rate function on each sub-fault, and are inverted simultaneously with

the observed surface offsets using a recently developed finite-fault inverse procedure (Ji et al., 2002b). Ours (Ji et al., 2002a) and other studies (Kikuchi and Yamanaka, 2002) indicate that the rupture initiated

as a thrust event before traveling southeast along 220 km of the Denali fault. Slip along this segment increased from 6 m in the northwest to more than 10 m in the southeast. During the later part of the earthquake the rupture branches off the Denali fault onto the Totichunda fault, where it continues in strike–slip fashion. To use the finite fault model in our numerical simulations we approximate it by a set of 475 sub-events of size  $4 \text{ km} \times 5 \text{ km}$ ; these sub-events represent the distribution of the moment–density tensor.

### 3. Spectral-element method

We use a spectral-element method (SEM) to simulate 3D global seismic wave propagation generated by this earthquake. The method incorporates 3D variations in compressional wave speed, shear-wave speed and density, attenuation, anisotropy, ellipticity, topography and bathymetry, and crustal thickness (Komatitsch and Vilotte, 1998; Chaljub, 2000; Komatitsch et al., 2002; Komatitsch and Tromp,

2002a,b). We use model S20RTS of the mantle (Ritsema et al., 1999), model CRUST2.0 of the crust (Bassin et al., 2000), and topography and bathymetry model ETOPO5 (from the US National Oceanic and Atmospheric Administration). The SEM is implemented on the world’s fastest computer (<http://www.top500.org>): the Earth Simulator. The simulations are performed on 1944 processors, which require 243 out of 640 nodes of the Earth Simulator. We use a mesh with 82 million spectral-elements, for a total of 5467 million global integration grid points (i.e. almost 15 billion degrees of freedom) (Fig. 2). This translates into an approximate grid spacing of 2.9 km along the Earth’s surface. On this number of nodes, a simulation of 60 min of wave propagation accurate at periods of 5 s and longer requires about 15 h of CPU time. It should be noted that typical normal-mode summation codes that calculate semi-analytical synthetic seismograms for 1D spherically-symmetric Earth models (Dahlen and Tromp, 1998) are accurate up to 6 s. In other words, the Earth Simulator allows us to simulate global seismic

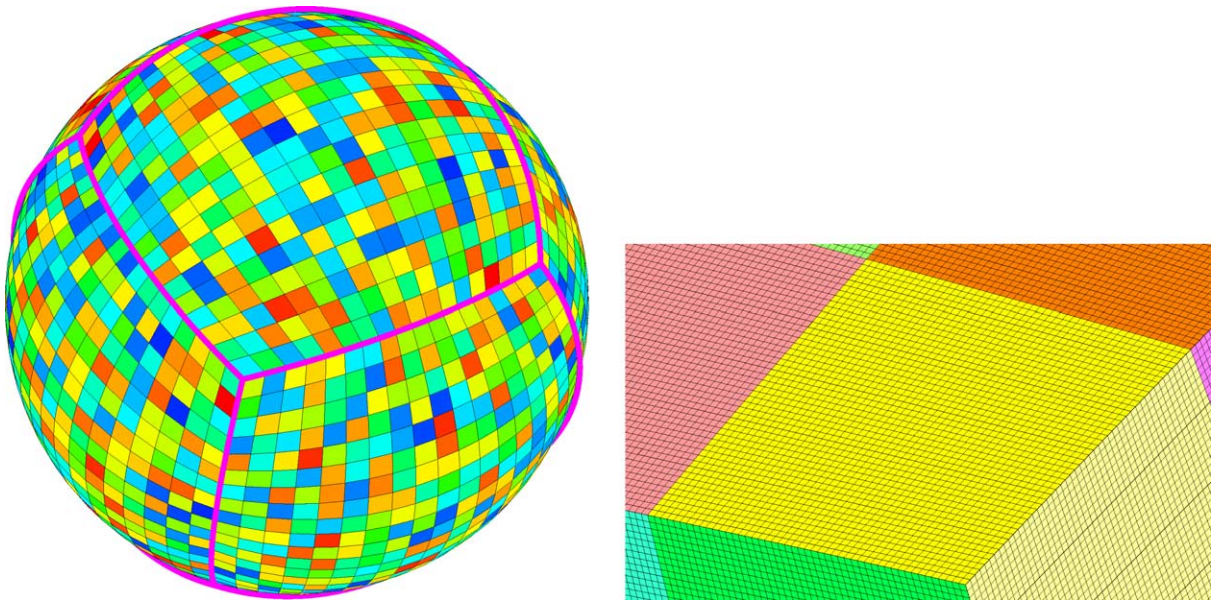


Fig. 2. The SEM uses a mesh of hexahedral finite elements on which the wave field is interpolated by high-degree Lagrange polynomials on Gauss–Lobatto–Legendre (GLL) integration points. The left figure shows a global view of the mesh at the surface, illustrating that each of the six sides of the so-called ‘cubed sphere’ mesh (Sadourny, 1972; Chaljub, 2000; Komatitsch and Tromp, 2002a) is divided into  $18 \times 18$  slices, shown here with different colors, for a total of 1944 slices. The right figure shows a close-up of the mesh of  $48 \times 48$  spectral-elements at the surface of each slice. Within each surface element we use  $5 \times 5 = 25$  GLL points, which translates into an average grid spacing of 2.9 km.

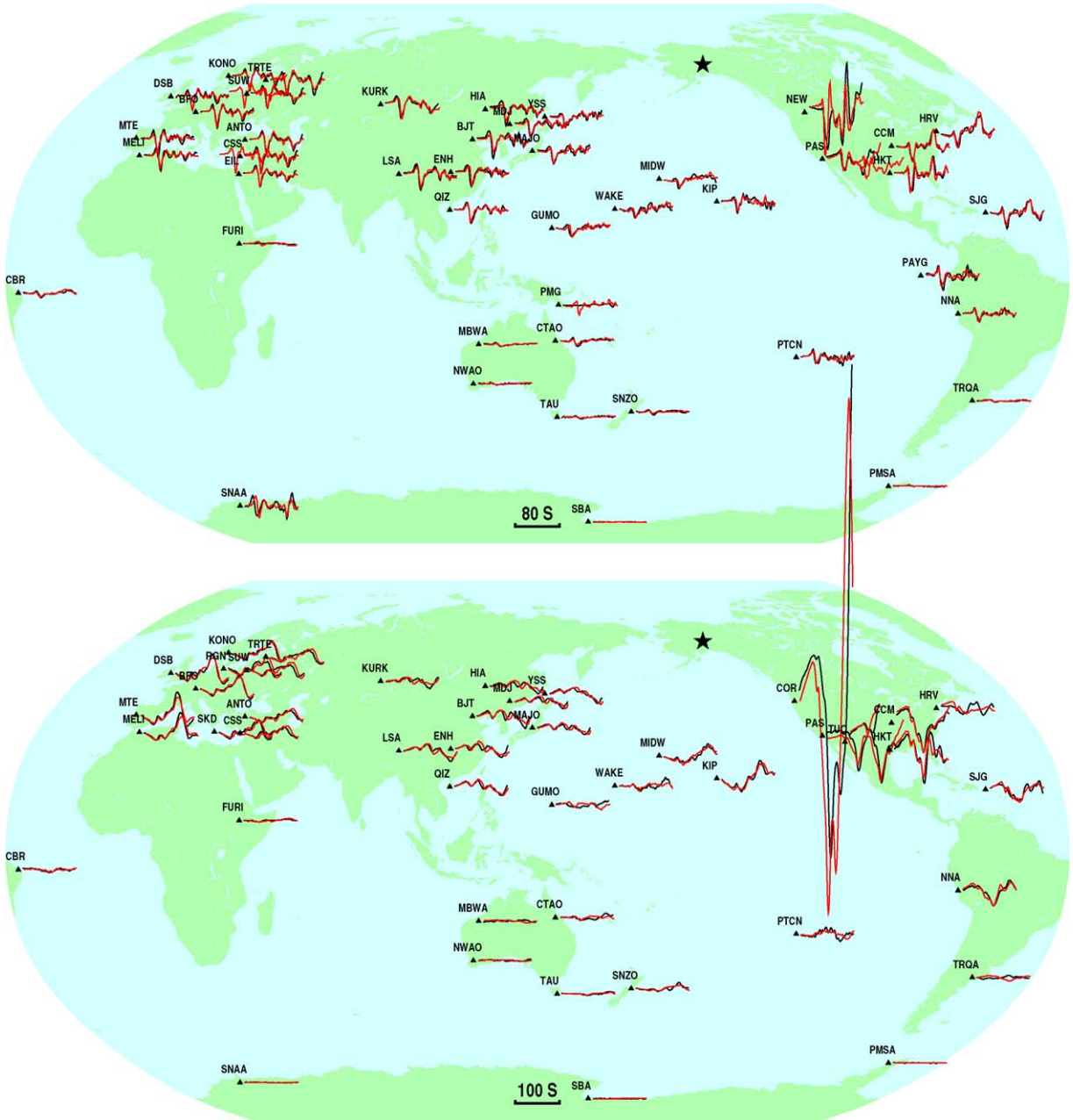


Fig. 3. Maps on which stations in the global seismographic network are labeled and denoted by black triangles. To the right of each station the data are shown in black and the 3D SEM synthetic seismograms in red. Both data and synthetic seismograms are bandpass-filtered with a two-pass six-pole Butterworth filter between periods of 5 and 150 s. The black star denotes the epicenter, and the black bar at the bottom denotes the time scale. Both data and synthetic seismograms are multiplied by the inverse of the body-wave geometrical spreading factor in an attempt to remove effects associated with epicentral distance. (Top) P-wave displacement on the vertical component. (Bottom) S-wave displacement on the transverse component. To compare the P- and S-wave amplitudes in the two figures the S-waves need to be multiplied by a factor of four.

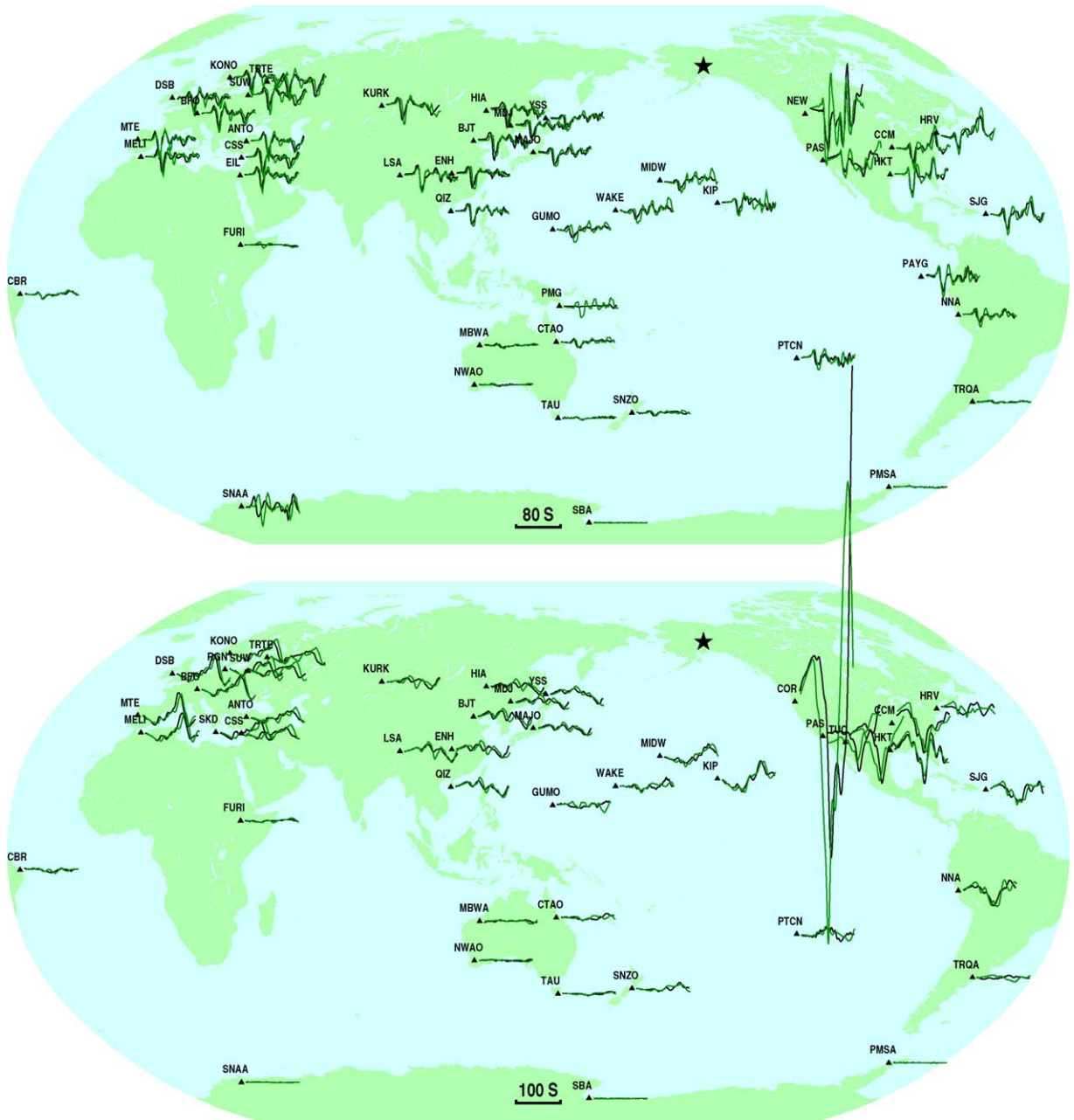


Fig. 4. Same as Fig. 3, except that the SEM synthetic seismograms, shown in green, are for the spherically symmetric 1D Earth model PREM (Dziewonski and Anderson, 1981). Generally, PREM synthetic seismograms are calculated based upon normal-mode summation (Dahlen and Tromp, 1998), which is a semi-analytical technique valid only for spherically symmetric Earth models. Because of the short-periods involved in the calculations presented here, mode catalogues are neither practical nor available, and thus the PREM synthetic seismograms were also calculated on the Earth Simulator based upon the SEM. (Top) P-wave displacement on the vertical component. (Bottom) S-wave displacement on the transverse component. To compare the P- and S-wave amplitudes in the two figures the S-waves need to be multiplied by a factor of four.

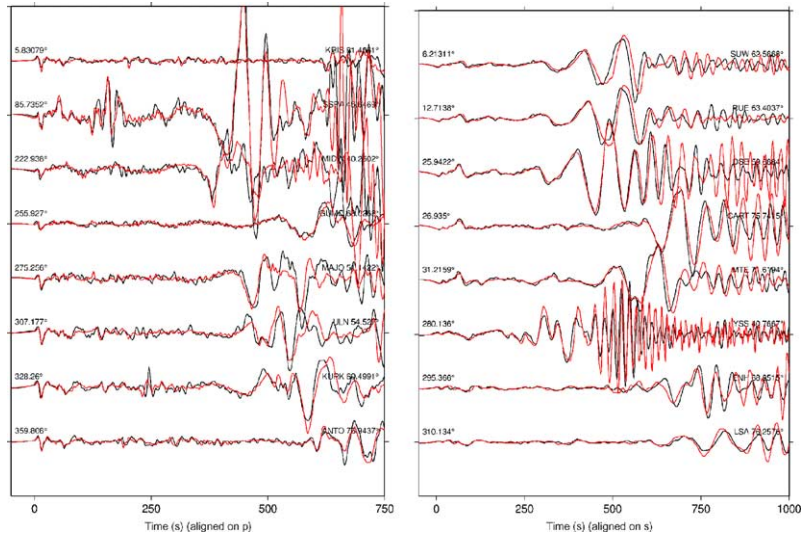


Fig. 5. Broadband data and synthetic displacement seismograms bandpass-filtered with a two-pass four-pole Butterworth filter between periods of 5 and 150 s. (Left) Vertical component data (black) and synthetic (red) displacement seismograms aligned on the arrival time of the P-wave. (Right) Transverse component data (black) and synthetic (red) displacement seismograms aligned on the arrival time of the S-wave. For each set of seismograms the azimuth is plotted above the records to the left, and the station name and epicentral distance are plotted to the right. The transverse component seismograms need to be multiplied by a factor of 10 to compare them directly with the vertical component seismograms.

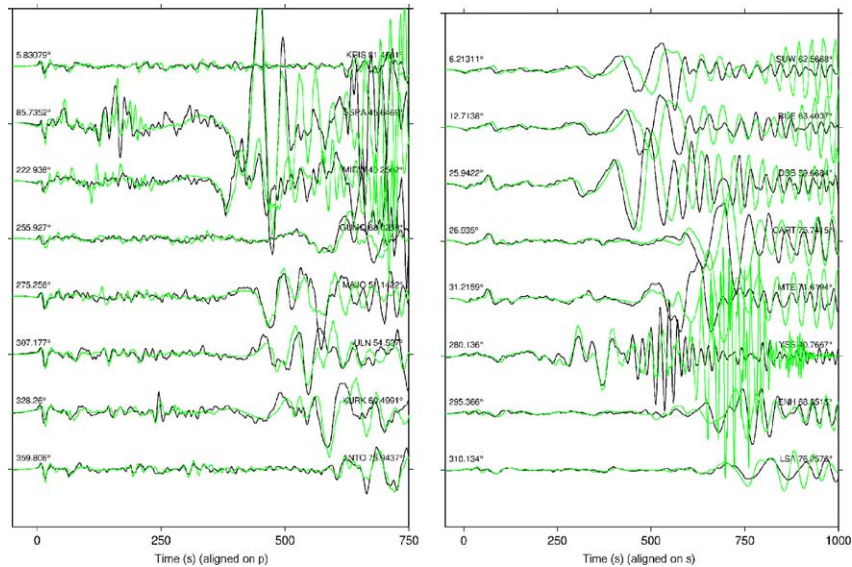


Fig. 6. Broadband data and 1D (PREM) synthetic displacement seismograms bandpass-filtered with a two-pass four-pole Butterworth filter between periods of 5 and 150 s. (Left) Vertical component data (black) and PREM synthetic (green) displacement seismograms aligned on the arrival time of the P-wave. (Right) Transverse component data (black) and PREM synthetic (red) displacement seismograms aligned on the arrival time of the S-wave. For each set of seismograms the azimuth is plotted above the records to the left, and the station name and epicentral distance are plotted to the right. The transverse component seismograms need to be multiplied by a factor of 10 to compare them directly with the vertical component seismograms.

wave propagation in fully 3D Earth models at periods shorter than current seismological practice for 1D spherically symmetric models. The SEM algorithm takes advantage of the unique hardware architecture of the Earth Simulator by combining parallel programming based upon communication between processors using message-passing (more specifically the message-passing interface MPI by Gropp et al. (1994)) and loop vectorization to use the vectorial structure of each processor efficiently.

#### 4. Results

In Fig. 3, we show the results of the simulation for compressional (P) and shear (S) waves at periods between 5 and 150 s. The largest P- and S-wave arrivals are observed in North America; this is due to the fact that the main rupture is in a south-easterly direction. The duration of the rupture is about 100 s (Fig. 1). The initial portion of the P-waveforms, in particular at European stations, reflects the thrust event that initiated the earthquake. The importance of 3D structure is illustrated by comparing the results in Fig. 3 with those in Fig. 4, which shows P- and S-wave data and synthetic seismograms for the one-dimensional (1D) spherically-symmetric Preliminary Reference Earth Model (PREM) by Dziewonski and Anderson (1981). The finite source model is the same for the 3D and PREM synthetic seismograms, so the differences are due to 3D heterogeneity. The overall P- and S-waveforms for PREM have the right shape, but the arrival times are off, which is an imprint of 3D heterogeneity in the mantle. In particular, P-waveforms recorded at Pacific stations, such as MIDW (Midway), KIP (Kipapa, Hawaii), WAKE (Wake Island), GUMO (Guam, Mariana Islands), and PTCN (Pitcairn Island), are fit much better by the 3D model. The same is true for S-waveforms recorded in Eurasia. S-waveforms in Europe, e.g. stations DSB (Dublin, Ireland), BFO (Black Forest, Germany), MTE (Manteigas, Portugal), and MELI (Melilla, Spain), clearly illustrate significant moment release toward the end of the rupture, a reflection of the moment release plotted in Fig. 1. Notice that both P- and S-waveforms are nearly nodal in Australia, something that is well captured by the finite source model. The huge S-wave at station COR (Corvallis, Oregon, USA) arrives 8 s too early in the

3D simulations. Apparently, the highly heterogeneous path along the west coast of North America is not slow enough in the 3D mantle model to explain the observed arrivals. Notice in Fig. 4 that the situation is even worse for spherically symmetric model PREM, in which the S-wave arrives 11 s too early at COR.

To illustrate the broadband nature of the seismograms, Fig. 5 shows 12 min of vertical component displacement seismograms starting at the arrival time of the P-wave, and 17 min of transverse component displacement seismograms starting at the arrival time of the S-wave. The transverse component of displacement has an amplitude that is 10 times larger than the vertical component. This reflects the predominantly strike-slip nature of the event. For reference, the same data are compared against SEM synthetics for 1D model PREM in Fig. 6. In particular the transverse component is fit significantly better by the 3D model.

#### 5. Discussion

The results in this article demonstrate that, given a detailed source model, good models of the mantle and crust, a precise numerical technique, and a sufficiently large computer, seismic signals that span an amplitude range that covers several orders of magnitude and a few decades in frequency can be accurately modeled. The fact that short-period synthetic seismograms based upon a degree-20 3D mantle model fit the observations reasonably well indicates that the overall picture of mantle heterogeneity is captured by current 3D tomographic inversions. It is intriguing that P-wave arrival times are also modeled well by the 3D P-wave model, which is obtained from the 3D S-wave model using a depth-dependent scaling factor,  $R = \delta \ln(\beta) / \delta \ln(\alpha)$ , which increases linearly from 1.3 at the surface to 3.0 at the core-mantle boundary, where  $\beta$  is the shear velocity and  $\alpha$  is the compressional velocity. Detailed study of the depth dependence of this scaling factor should give important insight into the material properties of the mantle. The broadband synthetic waveforms show that a finite source model can be used to simulate the directivity of both body and surface waves, and could ultimately be used in the inversion for complex source processes during large earthquakes. Such simulations can take into account the fact that many large earthquakes

occur in subduction zones, where the seismic velocity structure is highly heterogeneous due to the presence of the subducting oceanic plate.

Because our 3D synthetic seismograms provide a significant improvement in the fit to the data compared to synthetics for 1D models, they could be calculated routinely to provide a catalogue of 3D reference synthetics. The remaining differences between the data and these reference synthetics could be used as a starting point for further refining 3D Earth models.

### Acknowledgements

All the simulations were performed at the Earth Simulator Center of JAMSTEC by S.T. We thank Brian Savage for providing software that plots seismograms on maps. Broadband seismograms used in this study were recorded by IRIS Global Seismographic Network and obtained through the IRIS Data Management Center. Three of the authors (D.K., C.J. and J.T.) were funded in part by the US National Science Foundation. S.T. was funded by Grant-in-Aid for Scientific Research (KAKENHI 13640426) from Japan Society for the Promotion of Science.

### References

- Bassin, C., Laske, G., Masters, G., 2000. The Current Limits of Resolution for Surface Wave Tomography in North America. *EOS Trans. AGU*. 81: Fall Meet. Suppl., Abstract S12A-03.
- Chaljub, E., 2000. Modélisation numérique de la propagation d'ondes sismiques en géométrie sphérique: application à la sismologie globale (Numerical modelling of the propagation of seismic waves in spherical geometry: applications to global seismology). PhD thesis. Université Paris VII Denis Diderot, Paris, France.
- Dahlen, F.A., Tromp, J., 1998. *Theoretical Global Seismology*. Princeton University Press, Princeton.
- Dziewonski, A.M., Anderson, D.L., 1981. Preliminary reference Earth model. *Phys. Earth Planet. Inter.* 25, 297–356.
- Eberhart-Phillips, D., Haeussler, P.J., Freymueller, J.T., Frankel, A.D., Rubin, C.M., Craw, P., Ratchkovski, N.A., Anderson, G., Carver, G.A., Crone, A.J., Dawson, T.E., Fletcher, H., Hansen, R., Harp, E.L., Harris, R.A., Hill, D.P., Hreinsdottir, S., Jibson, R.W., Jones, L.M., Kayen, R., Keefer, D.K., Larsen, C.F., Moran, S.C., Personius, S.F., Plafker, G., Sherrod, B., Sieh, K., Sitar, N., Wallace, W.K., 2003. The 2002 Denali fault earthquake, Alaska: a large magnitude, slip-partitioned event. *Science* 300, 1113–1118.
- Engdahl, E.R., van der Hilst, R., Buland, R., 1998. Global teleseismic earthquake relocation with improved travel times and procedures for depth determination. *Bull. Seismol. Soc. Am.* 88, 722–743.
- Gropp, W., Lusk, E., Skjellum, A., 1994. *Using MPI, Portable Parallel Programming with the Message-Passing Interface*. MIT Press, Cambridge.
- Ji, C., Helmberger, D.V., Wald, D.J., 2002a. Preliminary Slip History of the 2002 Denali Earthquake. *EOS Trans. AGU*. 83: Fall Meet. Suppl., Abstract S72F-1344.
- Ji, C., Wald, D.J., Helmberger, D.V., 2002b. Source description of the 1999 Hector Mine, California earthquake. Part I. Wavelet domain inversion theory and resolution analysis. *Bull. Seismol. Soc. Am.* 92, 1192–1207.
- Kikuchi, M., Yamanaka, Y., 2002. Source rupture process of the central Alaska earthquake of November 3, 2002, inferred from teleseismic body waves. ERI, University of Tokyo, Japan. [http://www.eri.u-tokyo.ac.jp/EIC/EIC\\_News/021103AL-e.html](http://www.eri.u-tokyo.ac.jp/EIC/EIC_News/021103AL-e.html).
- Komatitsch, D., Vilotte, J.P., 1998. The spectral-element method: an efficient tool to simulate the seismic response of 2D and 3D geological structures. *Bull. Seismol. Soc. Am.* 88, 368–392.
- Komatitsch, D., Tromp, J., 2002a. Spectral-element simulations of global seismic wave propagation-I. Validation. *Geophys. J. Int.* 149, 390–412.
- Komatitsch, D., Tromp, J., 2002b. Spectral-element simulations of global seismic wave propagation-II. 3-D models, oceans, rotation, and self-gravitation. *Geophys. J. Int.* 150, 303–318.
- Komatitsch, D., Ritsema, J., Tromp, J., 2002. The spectral-element method, Beowulf computing, and global seismology. *Science* 298, 1737–1742.
- Page, R.A., Plafker, G., Pulpan, H., 1995. Block rotation in east-central Alaska: a framework for evaluating earthquake potential? *Geology* 23, 629–632.
- Ritsema, J., Van Heijst, H.J., Woodhouse, J.H., 1999. Complex shear velocity structure imaged beneath Africa and Iceland. *Science* 286, 1925–1928.
- Sadourny, R., 1972. Conservative finite-difference approximations of the primitive equations on quasi-uniform spherical grids. *Monthly Weather Rev.* 100, 136–144.